FORSCHUNGSZENTRUM
ROSSENDORF e.V.

FZR

FZR-69
Januar 1995
Preprint

S.M. Reimann, S. Frauendorf and M. Brack

Triaxial Shapes of Sodium Clusters

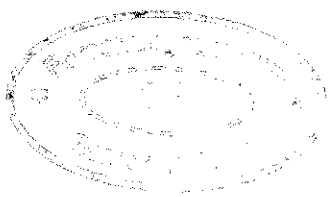

Forschungszentrum Rossendorf e.V.
Postfach 51 01 19 · D-01314 Dresden
Bundesrepublik Deutschland

Telefon (0351) 591 3261
Telefax (0351) 591 3700
E-Mail frauendorf@gamma.fz-rossendorf.de

TPR95-1

TRIAXIAL SHAPES OF SODIUM CLUSTERS

S.M. Reimann[1], S. Frauendorf[2], M. Brack[1]

[1] *Institut für Theoretische Physik, Universität Regensburg*
D–93040 Regensburg, Germany

[2] *Institut für Kern- und Hadronenphysik, Forschungszentrum Rossendorf e.V.,*
PF 510119, D–01314 Dresden, Germany

Abstract

A modified Nilsson-Clemenger model is combined with Strutinsky's shell correction method. For spherical clusters, the model potential is fitted to the single-particle spectra obtained from selfconsistent Kohn-Sham calculations. The deformation energy surfaces of sodium clusters with sizes of up to $N = 270$ atoms are calculated for a combination of triaxial, quadrupole and hexadecapole deformations. The ground state shapes and energies are determined by simultaneous minimization with respect to the three shape parameters. A significant fraction of the clusters is predicted to be triaxial. The deviations from the axial shape do not generate any systematic odd-even staggering of the binding energies.

PACS 36.40; 35.20.Wg; 71.45.Nt

1. INTRODUCTION

Shell structure in alkali metal clusters has been demonstrated experimentally for the first time by Knight *et al.* [1]. In sodium cluster beam experiments, they found enhanced abundances at the so-called "magic numbers" $N = 8, 20, 40, 58, 92, ...$ of valence electrons, which were predicted theoretically by Ekardt [2] and Beck [3] in the same year. Clemenger was the first to interpret the fine structure in the mass spectra of Ref. [1] between the magic numbers by spheroidal deformations [4], using a modified Nilsson Hamiltonian [5] in close analogy to the methods of nuclear physics. Like nuclei, clusters with closed shells have a spherical shape in most cases. When a shell is only partially filled, the system tends to stabilize itself by spontaneously breaking its symmetry, leading to a splitting of the highly degenerate spherical energy levels. According to the Jahn-Teller effect [6], the resulting subshell structure then leads to enhanced cluster stabilities between the spherical shell closings.

During the last years, cluster deformations have been extensively studied using various techniques (for a recent review, see Ref. [7]). For clusters with $N \leq 40$, the results of Clemenger's phenomenological model have been confirmed by self-consistent Kohn-Sham (KS) calculations in the jellium model [8, 31], which for axial symmetry recently have also been extended to the inclusion of hexadecapole and octupole deformations [9].

The effects of the discrete ionic structure have been treated explicitly in Refs. [10, 11, 12], but due to the numerical efforts inherent these methods, up to now they are only applicable to the smallest systems with $N \lesssim 20$.

Using Strutinsky's shell correction method [13], spheroidal [14] and more general axial shapes [15, 16] of sodium clusters have been determined for cluster sizes up to $N = 800$ atoms. A systematic study of cluster deformations with simultaneous minimization of five-dimensional multipolarity is given in Ref. [17], where a deformed Woods-Saxon potential is used. For a particle in a cavity, spheroidal deformations of very large systems with $N \lesssim 3000$ have been investigated in Ref. [18].

In general, the results of the different approaches mentioned above are quite similar. The results obtained from more sophisticated self-consistent calculations [9] agree qualitatively well with the Woods-Saxon (WS) calculations of Ref. [15, 17], as well as with the KS-Nilsson model (KSN) of Ref. [14]. This strongly supports the application of the shell-correction method to larger cluster sizes, where up to now the self-consistent methods are far too time-consuming.

Triaxial reflection symmetric shapes have been studied within the harmonic oscillator model [19, 22] as well as by means of the self-consistent local density jellium calculations [23]. These calculations are restricted to the lightest clusters below $N = 50$. In the present article, we extend the spheroidal KS-Nilsson model of Ref. [14] to the calculation of non-axial shapes of cluster sizes up to $N = 270$.

2. THE KOHN-SHAM-NILSSON METHOD

The main idea of the KS-Nilsson model (KSN) suggested in Ref. [14] is to combine the self-consistent KS calculations for spherical systems with the Nilsson Hamiltonian, which has a simple deformation dependence that facilitates the numerical calculations appreciably. The Hamiltonian is constructed such that in the spherical limit it approximates very closely the single-particle spectra of the KS calculations using the jellium model and the local density approximation.

We start from the single-particle Hamiltonian

$$\begin{aligned} H = H_{h.o.} &- \hbar\omega_0(N_0)\cdot U(N_0)\cdot \mathbf{l}^2 \\ \text{with}\quad H_{h.o.} &= T + \frac{1}{2}\hbar\omega_0(N_0)\cdot\rho^2\cdot\left\{1 - \frac{2}{3}\varepsilon_2\sqrt{\frac{4\pi}{5}}\cos\gamma\cdot Y_{20} + \right. \\ &+ \frac{2}{3}\varepsilon_2\sqrt{\frac{4\pi}{10}}\cdot\sin\gamma\,(Y_{22}+Y_{2-2}) + \\ &+ 2\varepsilon_4\left[\cos^2(3\gamma/2) + \frac{3}{8}\sin^2(3\gamma/2)\right]Y_{40} - \\ &- 2\varepsilon_4\frac{\sqrt{10}}{8}\sin^2(3\gamma/2)\,(Y_{42}+Y_{4-2}) + \\ &+ \left. 2\varepsilon_4\frac{\sqrt{70}}{16}\sin^2(3\gamma/2)(Y_{44}+Y_{4-4})\right\}, \end{aligned} \tag{1}$$

where ρ is the radius vector in triaxially stretched coordinates

$$\rho^2 = \sum_i \chi_i^2 \qquad \text{with} \quad \chi_i = x_i\cdot\sqrt{\frac{M\omega_i}{\hbar}}, \qquad i = 1,2,3\,, \tag{2}$$

which are defined by the anisotropic oscillator basis with the three frequencies

$$\omega_i = \omega_0\left(1 - \frac{2}{3}\varepsilon_2\cos\left(\gamma + \frac{2\pi}{3}\,i\right)\right), \qquad i = 1,2,3. \tag{3}$$

The potential parameters ω_0 and U depend on the spherical oscillator quantum number N_0 (see below). The hexadecapole part of the potential is chosen as a smooth interpolation between the prolate ($\gamma = 0°$) and the oblate axis ($\gamma = 60°$). The Hamiltonian (1) with an additional spin-orbit term has been used in nuclear physics in order to study the fission barriers for heavy elements by Larsson *et al.* [24].

As the potential is reflection symmetric, the parity $\Pi = (-1)^{N_0}$ is a good quantum number, and there are no couplings between even and odd N_0. It has been shown in the original work by Nilsson [5] and later on for triaxial deformations by Larsson *et al.* [24], that in strechted coordinates the couplings of states differing by $\Delta N_0 = 2$ vanish. Furthermore we neglect the couplings $\Delta N_0 \geq 4$ between different oscillator shells, which is known [5, 24] to change the single-particle spacings only very slightly. Hence, we diagonalize the Hamiltonian (1) only within each major shell N_0, which simplifies the numerical calculations very efficiently. The oscillator frequency $\omega_0(N_0)$ in Eq. (1) is scaled such that the deformed equipotential surfaces confine a constant volume. For a more detailed description of the technical details we refer to [24] and [25].

The l^2–term in Eq. (1) yields an intermediate between a pure oscillator potential and a square well. In general, the parameter $U(N_0)$ depends on the oscillator quantum number N_0. Already the simple l^2-form of the Hamiltonian reproduces the spherical spectra of self-consistent KS calculations extremely well. It is therefore possible to determine $U(N_0)$ directly from the KS results and to obtain a close correspondence of the spherical spectrum of the Hamiltonian (1) with self-consistent KS calculations. The detailed procedure is given in Ref. [14], we recall here only the most important steps.

The starting point are the spherical KS levels $\varepsilon_n(l)$, which we obtain from a density-functional calculation using the spherical jellium model and the local density approximation [26]. In Fig. 1 we show the KS energies (circles) for the cluster Na_{228} as an example. Each state is labeled by the corresponding values of the radial quantum number n and angular momentum l. The squares denote the single-particle energies used in the KSN. For Na_{228}, the Fermi energy ε_f lies between the $1k$ and $3f$–level, as marked in the diagram. From the l-dependence of the spherical eigenvalues we see that the exact KS levels, whose quantum numbers (n, l) belong to the same oscillator shell $N_0 = 2n - 1 + l$, lie approximately on straight lines. Therefore, the parameter U can be determined by a linear regression, where the value of $(\hbar\omega)(N_0)$

is given in Eq. (4) below.

For large deformations, some of the levels belonging to rather high shells come below the Fermi surface. Moreover, levels from several shells above the Fermi surface are needed in the Strutinsky averaging procedure. This necessitates the continuation of the spectra to energies $\varepsilon \gg \varepsilon_f$ even into the positive energy region. The finite depth of the KS potential, however, does not allow to calculate these levels. In Ref. [14] the spectrum is continued by the deformed oscillator states, describing asymptotic behavior of the Nilsson single-particle energies for large deformations. In the present work we found it better to extrapolate the KS levels to the continuum. We proceed as follows: The lowest eigenvalue in each oscillator shell N_0 has the radial quantum number $n = 1$. These states have the energy $\varepsilon_{(n=1)}(l)$ and are connected by the full drawn line in Fig. 1. We extrapolate the function $\varepsilon_{(n=1)}(l)$ linearly to higher quantum numbers $n = 1$ and $l = l^f + i$ with $i = 1, 2, 3, ...$, where l^f denotes the angular momentum of the *highest* energy level with $n = 1$ that has been calculated in the spherical KS potential. The levels with $n \neq 1$ are then given by the slopes $\hbar\omega_0(N_0)U(N_0)$ for each oscillator shell N_0. This method is very efficient in giving well-developed plateaus for the Strutinsky renormalisation, which enhances the accuracy of our method especially for smaller clusters. The overall energy scale of the potential is determined by the value of $\hbar\omega_0(N_0)$. In order to adjust it to the scale of the KS spectrum, we relate it to the corresponding mean square radius. For a given quantum number N_0 the virial theorem for the harmonic oscillator yields

$$\hbar\omega_0(N_0) = \frac{\hbar^2(N_0 + 3/2)}{M\langle r^2\rangle(N_0)}. \tag{4}$$

In Eq. 4 we use the averaged quantity $\langle r^2\rangle(N_0)$ in each oscillator shell N_0, where the value of $\langle r_\tau^2\rangle$ given by the KS calculations is weighted with its spherical degeneracy.

The cluster shapes are generated by the three deformation parameters $\varepsilon_2, \varepsilon_4$ and γ. Hereby, the two axial parameters ε_2 and ε_4 fix the quadrupole and hexadecapole deformations. The triaxiality parameter γ describes non-axial deformations, where $\gamma = 0°$ corresponds to *prolate* and $\gamma = 60°$ to *oblate* cluster shapes. For axial shapes the hexadecapole term describes the waist-line development. For triaxial deformations the parameterization interpolates smoothly between the shapes at $\gamma = 0°$ and $\gamma = 60°$. Note that following the "Lund convention", the sign of ε_4 is chosen opposite to the parameterization used in Refs. [15, 17, 9]. Reflection asymmetric shapes are not studied in the present paper; we refer to the work in Refs. [15, 17, 9].

Fig. 2 shows the spectrum of the Hamiltonian (1) for Na_{86} as an example. In the left panel the axial quadrupole deformation ε_2 increases from zero to its equilibrium value $\varepsilon_2 \approx 0.2$. Accordingly, the spherical KS single-particle energies are shown at the left-hand side of the diagram. As soon as $\varepsilon_2 \neq 0$, the spherical degeneracy is broken. In case of axial symmetry, the projection Λ of the angular momentum on the z-axis is a good quantum number. For the moderate prolate deformations shown, Λ changes with ascending energy from 0 to the l-value of the spherical state the levels emanate from. The degeneracy $\mathcal{D}$ of the states changes from $\mathcal{D} = 2(2l+1)$ in the spherical case to $\mathcal{D} = 2$ for $\Lambda = 0$ (spin orientation) and $\mathcal{D} = 4$ for $\Lambda \neq 0$ (spin orientation and sign of Λ), respectively. In the middle panel the hexadecapole deformation is turned on. As axial symmetry is maintained, the only influence of the ε_4-term is a shift in the position of the energy levels. The doublet-quartet structure in the degeneracies remains. On the right side of this panel ε_4 reaches its equilibrium value. In the right panel the triaxial deformation is switched on. Due to the breaking of the axial symmetry, Λ is no longer a constant of motion. The quartets (solid lines in the two left panels) appearing for axial shape are split and all states have only the two-fold spin degeneracy (dotted lines). There may be accidental degeneracies, but the states belonging to the same representation of the D_{2h} symmetry group of the Hamiltonian must not cross. The triaxial ground state deformation of Na_{86} is a clear consequence of the well-pronounced shell gap at $(\varepsilon_2, \varepsilon_4, \gamma) \approx (0.2, 0.1, 26)$ marked in the diagram. The deformation energy surface of Na_{86} is given in Fig. 3 below.

3. STRUTINSKY RENORMALISATION

In nuclear physics it has been well known for a long time that the sum over the lowest occupied single-particle energies fails to correctly describe the deformation energy of an interacting many-particle system. Therefore, we calculate the renormalized deformation energies by means of Strutinsky's "shell correction method" (SCM), which was initially developed for nuclear physics [13]. It has already been shown that this method is very efficient for the calculation of the ground state deformations of clusters in a very large size range, exploring a large class of axial shapes [15, 17, 14, 18]. We recall here only the very principles of the method and refer to Refs. [13, 27] for a more detailed discussion.

Considering the cluster as a quantal droplet, its total energy can be split up

into two parts: an average classical part, the so-called "liquid drop energy" (LDM), which is parameterized by a macroscopic expression, and a "shell correction energy", $\delta E(\varepsilon_2, \varepsilon_4, \gamma)$, which arises from the quantised electron motion inside the droplet. The latter is related to the variations of the density of states around the Fermi surface and can be determined from the total single particle energy E_{sp}, which is the sum of occupied levels

$$E_{sp} = \sum_{i=1}^{N} \varepsilon_i = \delta E + \widetilde{E}, \tag{5}$$

where $\widetilde{E}$ is given by

$$\widetilde{E} = \int_{-\infty}^{\varepsilon_f} E\, \widetilde{g}(E)\, \mathrm{d}E, \tag{6}$$

and ε_f corresponds to the Fermi energy. The average level density $\widetilde{g}(E)$ is defined by folding the exact quantum density of states $g(E)$

$$g(E) = \sum_{i=1}^{N} \delta(E - \varepsilon_i) \tag{7}$$

with a smooth distribution function $f_{2M}(x)$. Usually one takes a Gaussian of half-width $\Gamma \gtrsim \hbar\omega_0$ multiplied by a curvature correction polynomial. It is necessary to impose on $\widetilde{E}$ the stationary condition

$$\left(\frac{\mathrm{d}\widetilde{E}}{\mathrm{d}\Gamma}\right)_{(\Gamma=\Gamma_0)} = 0, \tag{8}$$

which is the differential form of the usual plateau condition, requiring that $\widetilde{E}$ does not depend on the averaging width Γ. We use a curvature correction polynomial of the order $2M = 6$ (cf. [27]), which fulfills the plateau condition with respect to Γ very well. In most cases a smoothing width of $\Gamma_{pl} \approx 1.2\hbar\omega_0$ is appropriate, where $\hbar\omega_0$ is the average of the values $\hbar\omega_0(N_0)$ belonging to the three oscillator shells N_0 around the Fermi level. The continuation of the spherical spectrum high above the Fermi energy suggested in this paper makes the plateaus more stable than the ones obtained in Ref. [14] for the spheroidal KSN, where high-lying energy levels are approximated by the anisotropic oscillator states. The plateaus are even acceptable for the light clusters $N \leq 30$, where it is generally expected that the uncertainties in the shell correction δE due to badly developed plateaus become significant. For the

accurate renormalisation it is important to include a sufficient number of shells. In our calculations, we have reached convergence of the shell corrections $\delta E(\varepsilon_2, \varepsilon_4, \gamma)$ for $N_0 < 16$.

To determine the equilibrium deformations for neutral clusters, we calculate the "shell energy"

$$E_{shell}(\varepsilon_2, \varepsilon_4, \gamma) = \Delta E_{surf} + \delta E(\varepsilon_2, \varepsilon_4, \gamma), \tag{9}$$

locating the zero point of the energy at the LDM energy for spherical shape. The surface energy ΔE_{surf} relative to the spherical drop is given by

$$\Delta E_{surf} = a_s \cdot (B_{surf}(\varepsilon_2, \varepsilon_4, \gamma) - 1) \cdot N^{2/3} \tag{10}$$

and depends on the cluster shape via the ratio $B_{surf}(\varepsilon_2, \varepsilon_4, \gamma)$ of the surface areas of the deformed and spherical clusters of the same volume. The surface area is calculated by numerical integration over the equipotential surface of the potential (1). The details are described in Refs. [24, 28]. The constant a_s is the bulk surface energy and is given by

$$a_s = 4\pi\sigma r_s^2, \tag{11}$$

where σ is the surface tension. We fix the surface energy in Eq. (10) to its experimental value, obtained from extrapolating the measured surface tension given in Ref. [29] to zero temperature. For a Wigner-Seitz radius $r_s = 3.96$ a.u., using the bulk value for σ this yields $a_s = 0.79$ eV, which is not too different from the melting point value. Following the arguments given in Ref. [17], curvature terms are neglected in the present calculations. The temperature of the valence electrons is taken to be zero. It has been shown in Ref. [30] that the shapes of light clusters with $N \lesssim 100$ are not significantly modified by the thermal fluctuations, whereas the thermal averaging makes larger clusters around the magic numbers spherical.

4. RESULTS

The shell energy (9) is calculated as a function of the $(\varepsilon_2, \varepsilon_4, \gamma)$-degrees of freedom, generating a potential energy surface (PES) whose minima correspond to stable or metastable shapes of a cluster. The PES are constructed for triaxial deformations in the range $0^o \leq \gamma \leq 60^o$, where the quadrupole and hexadecapole deformations are varied between $0 \leq \varepsilon_2 \leq 0.7$ and $-0.2 \leq \varepsilon_4 \leq 0.2$.

As examples, we show in Fig. 3 the contours of the PES in the (ε_2, γ)–plane for the clusters with $N = 12, 14, 16, 28, 86, 132, 186$ and 228. Examples of the PES for axial quadrupole and hexadecapole deformations for larger clusters $N = 78, 112, 122$ and 154 are shown in Fig. 4. For each sodium cluster with $10 \leq N \leq 270$ valence electrons, we minimize the shell energy (9) *simultaneously* for the three deformation parameters $(\varepsilon_2, \varepsilon_4, \gamma)$. The results are presented in Fig. 5, showing the ground state deformations as a function of the cluster size N. Fig. 6 shows the separation energies and in Fig. 7 we compare the axial with the triaxial shell energies.

From Figs. 5-7 we see that strong spherical shells occur at N =20, (36), 58, 92, 38, 190 and 254, and subshells are found at N =78, 112, 122, 154, 162, 176 and 218.

In conformity with the results of the spheroidal KSN, the minimized quadrupole deformation $\varepsilon_2(N)$ is an almost periodic function, with its period given by the distance between the spherical shell closings (cf. Fig. 5). Deformations on the prolate side ($\gamma \leq 30°$) dominate, and most of the axial deformations on the oblate side found in Ref. [14] become triaxial. Similar trends are known from atomic nuclei. Larsson has already pointed out in Ref. [24] that the hexadecapole deformation usually lowers the energy on the prolate side more than on the oblate side.

Triaxial ground state deformations are most frequent at the beginning and the end of a shell. Strong triaxial deformations are found in the mass ranges 11–13, 15-17, 23-25, 61-65, 71–73, 81-86, 95-101, 105-107, 131-135 and 186-191. The triaxiality around 156 and 178 is very small ($\gamma \leq 7°$). Compared to the two-dimensional minimization of $(\varepsilon_2, \varepsilon_4)$-shapes the energy gain due to triaxiality may amount to be ≈ 0.2eV for the light clusters and $\lesssim 0.05$eV for the heavy ones (cf. Figs. 3, 7).

In Fig. 3 we show the contour diagrams of the PES in the (ε_2, γ)-plane for the clusters $N = 12, 14, 16, 28, 86, 132, 186$ and 228. The PES are calculated at the minimized hexadecapole ground state deformation ε_4 in each mesh point. For Na_{12}, the PES shows a single pronounced triaxial minimum at the ground state deformation $(\varepsilon_2, \varepsilon_4, \gamma) = (0.52, -0.03, 32°)$, which is separated from the oblate axial saddle at $(\varepsilon_2, \varepsilon_4, \gamma) = (0.43, -0.03, 60°)$ by ≈ 0.2eV. For Na_{14}, the prolate ground state at $(\varepsilon_2, \varepsilon_4, \gamma) = (0.51, 0.17, 0°)$ and the oblate isomeric state at $(\varepsilon_2, \varepsilon_4, \gamma) = (0.5, -0.12, 60°)$ are both stable with respect to triaxiality, and the saddle between the prolate and oblate minimum is moved into the γ-plane. The PES of Na_{16} has a minimum slightly more on the oblate side $(\varepsilon_2, \varepsilon_4, \gamma) = (0.48, 0.09, 37°)$ and shows a prolate isomer at $(\varepsilon_2, \varepsilon_4, \gamma) = (0.35, 0.08, 0°)$, separated from the triaxial

ground state by a barrier of ≈ 0.1eV. Full KS calculations of non-axial asymmetric quadrupole deformations without hexadecapole contributions [23] find triaxiality for Na_{12} and Na_{16}, too. In the KSN, the clusters Na_{10}, Na_{14} and Na_{18} are found to be axially symmetric. This agrees with the KS results of Ref. [9], which calculates the PES of singly charged sodium clusters with $10 \leq Z \leq 44$ valence electrons for $(\varepsilon_2, \varepsilon_3, \varepsilon_4)$–shapes in the structurally averaged jellium model. The PES of quadrupole and hexadecapole deformations for axial shapes ($\gamma = 0°, 60°$) are found to be very similar to the KS results in a range $N \lesssim 30$ [32]. In the "ultimate jellium model" of Koskinen *et al.* [33], one finds that the clusters with $N = 14, 21, 22$ have both axial and reflection symmetry, whereas Na_{10} is found to be axial, but asymmetric. Wholly unsymmetrical are the clusters with $N = 12, 16, 17, 18$. For Na_{28}, we find a prolate minimum at $(\varepsilon_2, \varepsilon_4, \gamma) = (0.34, 0.04, 0°)$, and a triaxial isomer at $(\varepsilon_2, \varepsilon_4, \gamma) = (0.36, 0.03, 18°)$. The oblate isomer is found at at $(\varepsilon_2, \varepsilon_4, \gamma) = (0.35, -0.17, 60°)$. Like for Na_{14}, we find that allowing for triaxiality lowers the barrier between the axial isomers.

The spherical shell of Na_{40} is not correctly described in our KSN. We obtain a weak closure at 36 instead. The reason is the position of the $1f, 2p$ and $1g$ levels in the KS spectra for sharp edge jellium, which gives a too small shell gap between $2p$ and $1g$ (see Ref. [7] and Refs. quoted therein). Montag et al. [9] use for the KS potential a diffuse surface of the ionic density. They demonstrate that a change in the diffuseness has the largest effects around $N = 40$, where it increases the energy gap between the $2p$ and $1g$ level in the single-particle spectrum and, thus, reproduces the experimental observation of the magic number $N = 40$. Out of this critical region around 40 our KSN is in accordance with the KS results of Refs. [31, 9, 32].

The triaxiality of larger clusters is illustrated in the lower part of Fig. 3 which shows the (ε_2, γ)–planes of Na_{86}, Na_{132}, Na_{186} and Na_{228} for the minimized hexadecapole deformation in each mesh point. Generally, the PES have a tendency of decreasing quadrupole deformations and for $\varepsilon_2 \gtrsim 0.3$ almost no metastable minima are found. With increasing cluster size, the magnitude of the axial equilibrium deformations becomes smaller, what can be understood from the relative size of the shell correction and surface energy, which scale with $N^{1/3}$ and $N^{2/3}$, respectively. Axial deformations are found to be more frequent for the large clusters. For spheroidal deformations in the KSN, a systematics of shape transitions between two magic shells from spherical $\longrightarrow$ oblate $\longrightarrow$ prolate $\longrightarrow$ spherical has been found in Refs. [14, 15, 17, 18]. Motivated by the success of the Balian-Bloch theory [34] in

explaining the supershell structure [35] experimentally found in the cluster abundancies [36, 37], a semiclassical interpretation of the above deformation systematics in terms of the triangular and rhomboidal classical periodic orbits confined to a spheroidal cavity [38] has been given in Ref. [39], adopting the results from nuclear physics by Strutinsky *et al.* [13].

The PES for quadrupole and hexadecapole deformations of the clusters Na_{78}, Na_{112}, Na_{122} and Na_{154} are shown in Fig. 4. Inspection of the three-dimensional deformation space shows that all these clusters have axial shape, each with a pronounced minimum at the prolate side and a stable oblate isomer, lying slightly higher in energy. The energy differences $E_o - E_p$ between the two stable oblate and prolate isomers are given below each diagram, together with the corresponding shape parameters $(\varepsilon_2, \varepsilon_4)$. Generally we find for the larger clusters that the shape isomerism is much more pronounced in the $(\varepsilon_2, \varepsilon_4)$–plane than for triaxial deformations. This is a consequence of the fact that triaxiality leads to much smaller shifts of the single particle energies than the axial deformations.

In Fig. 6, we show the separation energies

$$\Delta_1 E(N) = E_{tot}(N-1) - E_{tot}(N) \tag{12}$$

calculated from the total energies

$$E_{tot}(N) = a_v \cdot N + a_s \cdot B_{surf}(\varepsilon_2, \varepsilon_4, \gamma) N^{2/3}, \tag{13}$$

where the first term corresponds to the bulk volume energy with $a_v = -1.12$eV. This value is obtained by extrapolating the bulk binding energies of liquid sodium, as given in Ref. [40], to zero temperature (for details cf. Refs. [17, 30]).

The major shell closings as well as the subshells clearly show up in the separation energies. The dominant structure already comes from the axial deformations ε_2 and ε_4. Triaxiality leads to small energy shifts that are barely seen in the separation energies (c.f. the comparison of axial $(\varepsilon_2, \varepsilon_4)$ and triaxial calculations $(\varepsilon_2, \varepsilon_4, \gamma)$ in the upper panel).

In Fig. 7, we compare the shell energies for the axial deformations (ε_2) and $(\varepsilon_2, \varepsilon_4)$ with the combination of axial and triaxial deformations (ε_2, γ) and $(\varepsilon_2, \varepsilon_4, \gamma)$. All triaxial PES are found to be very soft, and the energy differences between the axial and triaxial minima are in the most cases too small to show up on the scale of Fig. 7.

Comparing the two-dimensional minimizations $(\varepsilon_2, \varepsilon_4)$ and (ε_2, γ) with the one-dimensional minimization (ε_2) demonstrates clearly that it is the hexadecapole deformation that brings the important gain in binding energy. It may amount to 0.3eV at the beginning and the end of a shell. Our study shows that the binding energies calculated in Ref. [17] by minimizing a five dimensional family of axial shapes should be rather accurate and non axial shapes should modify these values only slightly.

Restrictions in the shape parameterization generally lead to an overestimation of the shell structure in the energies as function of the cluster size N. In Fig. 7 we see that the shell energies for one-dimensional minimization (ε_2) have higher energies as those with the hexadecapole deformations included $(\varepsilon_2, \varepsilon_4)$, what is most obvious at the beginning and the end of each shell. The hexadecapole deformation lowers these spikes in the deformed regions, just as the spheroidal deformation cuts away the huge shell maxima of the spherical clusters. Generally, with increasing variety of shapes, the N-dependence of the shell energies tends to become smoother. A semiclassical interpretation of these effects as well as an explanation of the higher multipole degrees of freedom in terms of the periodic orbit theory for the deformed clusters is of large interest [41].

Hamamoto *et al.* [42] used a modified oscillator potential for axial and non-axial quadrupole deformations to calculate the equilibrium deformations by minimizing the sum of the single particle energies. In qualitative agreement to the results shown above, they find that at the beginning of a major shell, oblate shapes are most favorable, whereas at the end of the shell prolate deformations are found. The number of clusters with a prolate minimum is much larger than that of oblate clusters, which is consistent with Fig. 5 of our calculations. Triaxiality is found between $N \approx 70$ and 75, between $N \approx 80$ and 85, around 105 and in the region between 152 and 158 (see Fig. 20 in Ref. [42]). The energy gain in shell energies by triaxial deformation turns out to be small, which confirms our results described above. In the region between 152 and 158 octupole deformations of the Y_{32}– type are found to be energetically more favorable than the triaxial quadrupole deformations.

5. EXPERIMENTAL CONSEQUENCES OF THE TRIAXIALITY

In order to find experimental quantities that are sensitive to the triaxiality of the cluster shape, we discuss the following possibilities: abundancies, the splitting of the plasmon resonance, separation energies and magnetic moments.

Comparing the separation- and deformation energies shown in Fig. 6 and Fig. 7 to the logarithmic derivatives of the experimental mass abundances of sodium clusters in Ref. [36, 37, 14] one finds that there is an obvious correlation of the most pronounced open-shell structures. In the experimental data of Refs. [36, 37, 14], between the "magic" shells broad low-amplitude dips occur at the cluster sizes $N \approx 66, 80, 116, 170$ and 240. In the present work as well as in the spheroidal KSN-model of Ref. [14] and the axial WS-calculations of Ref. [15, 17] the electron numbers $N = 72, 112, 172$ and 236 correspond to particularly stable configurations. The axial and triaxial results are found to be very similar. Thus, the shell structure in the deformation energies as well as the experimental abundance spectra seems to contain no obvious evidence for triaxiality (however, c.f. below the discussion of the odd-even staggering in the separation energies).

As already well known from nuclear physics and discussed in Ref. [19] for alkali clusters, the plasmon resonance is expected to split into three peaks of equal intensity if the shape is triaxial. The three resonances correspond to the eigenmodes along the three principal axes. Selby *et al.* [19] observe for the neutral cluster Na_{12} an absorption spectrum that seems to show three peaks. This agrees well with the calculated strong and stable triaxiality in our model as well as with previous calculations that also find triaxiality for this cluster [19, 23]. It also agrees with the microscopic RPA-calculation of the dipole resonance in Ref. [43]. The absorption cross sections for other neutral sodium clusters [19, 44] do not show enough structure to allow definite conclusions. The the plasmon resonance in singly charged clusters has been measured by Borggreen *et al.* [20]. They do not include N=12. For Na_{13} and Na_{14} a low intensity low frequency peak and a high intensity high frequency peak, characteristic for a prolate axial shape, is observed. We find Na_{13} to be triaxial with $(\varepsilon_2, \varepsilon_4, \gamma) = (0.51, 0.11, 10°)$, and for Na_{14} the prolate minimum is well separated from the oblate isomer by a barrier in the (ε_2, γ) - plane (cf. Fig. 3). For N=17 and 18 a high intensity low frequency and a low intensity high frequency peak is observed, characteristic for oblate shape. For N=15 and 16 a broad single resonance is seen that might correspond to three unresolved peaks. This would be in accordance with our calculations in Fig. 5 showing a transition from prolate to oblate shape with $N = 15$ and $N = 16$ being triaxial. For Na_{28} the axial calculations of Ref. [15, 17] find a prolate and an oblate minimum at almost the same energy, what may explain the experimental observation of two peaks of the same intensity

[20]. We find a PES for Na_{28} that has a prolate minimum and a triaxial isomer with almost no barrier between them, and the oblate isomer lies only slightly higher in energy. The coexistence of the prolate and triaxial minimum should result in the apperance of a third peak in the resonance.

The measurement of the plasmon resonance for the heavier clusters with predicted strong triaxiality, especially at $N = 64, 72$ and between 81 and 86 would be a strong test of our calculations.

The separation energies are expected to show different N–dependence for axial and triaxial shapes. As discussed in Ref. [17], the quartets of electron states originating from the $\Lambda \neq 0$ levels (the degeneracy is four because of the two orientation of the orbital angular momentum and the spin) show up in the plot $\Delta_1 E(N)$ as four points in a row on an upsloping almost straight line. For triaxial shapes there is only a two-fold degeneracy, which will cause an odd-even staggering of the separation energies, if the electron levels are well separated. It is seen in Fig. 6 that there are many quartets. This is partially due to the fact that many clusters are axial but also a consequence of the relatively small energy gain by triaxial deformation. The comparison of the axial with the triaxial calculation in the upper panel shows how for N =13 and N =23 the triaxiality generates a dip, thus destroying the corresponding quartets. The dip at N =17 is less pronounced. The experimental separation energies [21] and ionization potentials, however, show a *systematic* odd-even staggering that cannot be explained by the occurrence of triaxial quadrupole deformation for certain electron numbers, as found by our KSN calculations.

In Refs. [22, 33] it is demonstrated that the inclusion of a spin-dependent exchange-correlation potential in the KS calculations reduces the odd-even staggering by about 30% from the result of the spin-independent formalism. Recent calculations of even light clusters show that axial shapes with half-filled quartets, where the two electrons are in a triplet state, are energetically favoured by the spin-dependent exchange correlations according to Hund's rule [45].

Fig. 8 shows the orbital magnetic moments of the light clusters with odd N. The orbital part of the magnetic moment, measured in units of the Bohr magneton, is just equal to the expectation value of the orbital angular momentum component l_3. (The other two components are equal to zero.) As discussed in Ref. [16], this expectation value can only be nonzero if the cluster has an axial shape. For triaxial shape

the orbital magnetic moment is quenched[1]. By comparing the calculated orbital moments of the triaxial minimum to the one for the lowest axial saddle, Fig. 8 demonstrates that there is a number of clusters for which the triaxial deformation will quench the orbital paramagnetic moment. Since the energy gain by triaxial deformation is always large compared with the interaction energy with the external magnetic field ($\sim 10^{-4}$eV for a magnetic field of 1T), the field is too weak to restore the magnetic moment. It has been demonstrated by de Heer [46] that paramagnetic moments of the order of one Bohr magneton can be measured by deflection of the cluster beam in a strong Stern-Gerlach magnet. Such experiments could provide a rather direct evidence whether the cluster shape is axial or not.

5. CONCLUSIONS

In summary, we have shown that stable triaxial ground states exist for sodium clusters in a size range $N < 270$. The dominant effects in deformation energies, however, come from axially symmetric quadrupole and hexadecapole deformation, and triaxiality plays a minor role in the explanation of subshell closings in the abundance spectra. The splittings of the plasmon resonances seem to contain some evidence for triaxiality that may correlate with our predictions. However, the picture is far from being clear. Triaxiality modifies the N - dependence of the separation energies. The quartets, characteristic for axial shape, are disturbed and the odd-even staggering, characteristic for only two-fold spin-degenerated electron levels appears. However, a *systematic* odd-even staggering, as experimentally observed for the separation energies, the abundancies and the ionization potentials, cannot be reproduced by the calculations, since not all clusters are found to be triaxial and the energy for triaxial deformation is often too small to generate a significant perturbation. Thus, we conclude that the odd-even staggering has another origin. The measurement of the paramagnetic moments by deflection of the cluster beam in a magnet seems to be an interesting possibility to distinguish axial from non axial clusters, since finite orbital moments exist only for the symmetric species.

ACKNOWLEDGEMENTS

[1]The quenching of the orbital paramagnetic moment in a non-axial crystal field is a well known phenomenon in solid state physics.

Discussions with Th. Hirschmann, M. Rotter, V. Pashkevich and I. Hamamoto are gratefully acknowledged. We thank especially Th. Hirschmann for his invaluable help with the computer graphics and many numerical questions. We acknowledge financial support by the Commission of the European Communities (EC project ERB-SCI-CT92-0770) and the Deutsche Forschungsgemeinschaft for travel grants.

References

[1] Knight, W.D., Clemenger, K., de Heer, W.A., Saunders, W.A., Chou, M.Y., Cohen, M.L., Phys. Rev. Lett. **52**, 2141 (1984); Knight, W.D., Clemenger, K., de Heer, W.A., Saunders, W.A., Phys. Rev. B **31**, 2539 (1985)

[2] Ekardt, W., Phys. Rev. B**29**, 1558 (1984)

[3] Beck, D.E., Solid State Comm. **49**, 381 (1984)

[4] Clemenger, K., Phys. Rev. B**32**, 1359 (1985), and Ph. D. Thesis, Berkeley 1985 (unpublished)

[5] Nilsson, S.G., Mat.- Fys. Medd. Dan. Vidensk. Selsk. **29**, 16 (1955)

[6] Jahn, H.A., and Teller, E., Proc. Roy. Soc. London A**161**, 220 (1937)

[7] Brack, M., Rev. Mod. Phys. **65**, 677 (1993)

[8] Ekardt, W., and Penzar, Z., Phys. Rev. B**38**, 4273 (1988)

[9] Montag, B., Hirschmann, Th., Meyer, J., Reinhard, P.-G., Brack, M., Phys. Rev. Lett. 1994, in print.

[10] Röthlisberger, U., and Andreoni, W., J. Chem. Phys. **94**, 8129 (1991)

[11] Martins, J., Buttet, J., and Car, R., Phys. Rev. B**31**, 1804 (1985)

[12] Poteau, R., Spiegelmann, F., Phys. Rev. B**45**, 1878 (1992); J. Chem. Phys. **98**, 6540 (1993)

[13] Strutinsky, V.M., Sov. J. Nucl. Phys. **3**, 449 (1967), Nucl. Phys. A **95**, 420 (1967); *ibid.* A **122**, 1 (1968)

[14] Reimann, S.M., Brack, M., Hansen, K., Z. Phys. D **28**, 235 (1993)

[15] Frauendorf, S., and Pashkevich, V., Z. Phys. D**26**, 98 (1993)

[16] Frauendorf, S., Pashkevich, V., and Reimann, S.M. Contribution to the IS-SPIC7 in Kobe, Japan, (1994), Surface Letters and Reviews, in print (1995)

[17] Frauendorf, S., and Pashkevich, V., submitted to Phys. Rev. B (1994)

[18] Bulgac, A., and Lewenkopf, C., Phys. Rev. Lett. **71**, 4130 (1993)

[19] Selby, K., Vollmer, M., Masui, J., de Heer, W.A., Knight, W.D., Phys. Rev. B**40** (1989) 5417.

[20] Borggreen, J., Chowdhury, P., Kebaili, N., Lundsberg-Nielsen, N., Lützenkirchen, K., Nielsen, M.B., Pedersen, J., Rasmussen, H.D., Phys. Rev. B **48**, 23, 17507 (1993)

[21] Bréchignac, C., Cahuzac, Ph., Leygnier, J., Pflaum, R., Roux, J.Ph., and Weiner, J., Z. Phys. D**12** (1983) 199.

[22] Manninen, M., Mansikka-aho, H., Nishioka, H., Takahashi, Y., Z. Phys. D**31** (1994) 259

[23] Lauritsch, G., Reinhard, P.-G., Brack, M., Phys. Lett. A**160**, **179**(1991); Rotter, M. *et al.*, to be published.

[24] Larsson, S.E., Phys. Scripta **8**, 17 (1973); Larsson, S.E., and Leander, G., Physics and Chemistry of Fission, Rochester, NY, (IAEA, Vienna 1974) p.177; Leander, G., and Larsson, S.E., Nucl. Phys. A**239**, 93 (1975)

[25] Bengtsson, T., Ragnarsson, I., Aberg, S., Chap. 1 in Computational Nuclear Physics I, ed. by Langanke, K., Maruhn, J.A., and Koonin, S.E., Berlin, Heidelberg, New York: Springer 1992

[26] Genzken, O., and Brack, M., Phys. Rev. Lett. **67**, 3286 (1991); and Genzken, O., Ph. D. Thesis, Regensburg 1992 (unpublished)

[27] Brack, M., and Pauli, H.-C., Nucl. Phys. A**207**, 401 (1973); Brack, M., Nuclear Models, edited by Bengtsson, R. *et al.*, Wiley, 1993, p.345

[28] Hasse, R.W., and Myers, W.D., Geometrical Relationships of Macroscopic Nuclear Physics, Springer Series in Nuclear and Particle Physics, Berlin, Heidelberg, New York: Springer 1988

[29] Germer, D., and Mayer, H., Z. Phys. **210**, 391 (1968)

[30] Frauendorf, S., and Pashkevich, V., Contribution to the ISSPIC7 in Kobe, Japan (1994), Surface Letter and Reviews, in print; and to be published

[31] Hirschmann, Th., Brack, M., Meyer, J., Ann. Physik **3**, 336 (1994)

[32] Hirschmann, Th., private communication

[33] Koskinen, M., Lipas, P.O., and Manninen, M., Univ. of Jyväskylä preprint 1994

[34] Balian, R., and Bloch, C., Ann. of Phys. **63**, 592 (1971); **69**, 76 (1972)

[35] Nishioka, H., Hansen, K., and Mottelson, B.R., Phys. Rev. B **42**, 9377 (1990); Genzken, O., and Brack, M., Phys. Rev. Lett. **67**, 3286 (1991)

[36] Bjørnholm, S., Borggreen, J., Echt, O., Hansen, K., Pedersen, J., Rasmussen, H., Phys. Rev. Lett. **65**, 1627 (1990); Z. Phys. D**19**, 47 (1991)

[37] Pedersen, J., Bjørnholm, S., Borggreen, J., Hansen, K., Martin, T.P., Rasmussen, H.D., Nature **353**, 733 (1991)

[38] Strutinsky, V.M., Magner, A.G., Ofengenden, S.R., Døssing, T., Z. Phys. A **283**, 269 (1977)

[39] Reimann, S.M., and Brack, M., J. Comp. Mat. Sci. **2**, 433 (1993)

[40] Knacke, O., Kubaschewski, O., Hesselmann, K., Thermochemical Properties of Inorganic Substances II, Berlin, Heidelberg, New York: Springer 1991, p. 1314.

[41] Magner, A.G. *et al.*, to be published.

[42] Hamamoto, I., Mottelson, B.R., Xie, H., Zhang, X.Z., Z. Phys. D**21**, 163 (1991)

[43] Bernath, M., *et al*, Phys. Lett. A**156** (1991) 307

[44] Selby, K., Kresin, V., Masui, J., Vollmer, M., de Heer, W.A., Scheidemann, A. , Knight, W., Phys. Rev. B**43** (1991) 4565.

[45] Kohl, C. *et al.*, to be published

[46] de Heer, W.A., Thesis, University of California, Berkeley, 1985

Figure Captions

Figure 1:
Single-particle energies of the self-consistent spherical KS energies (circles) and spherical energy levels of the KSN model (squares) as a function of $l(l+1)$, where l corresponds to the spherical angular momentum. The corresponding radial quantum numbers n and angular momenta l, as well as the Fermi surface and the function $\varepsilon_{n=1}(l)$ are given in the diagram. (We use the nuclear physics convention for the radial quantum numbers n).

Figure 2:
Nilsson single-particle energies for quadrupole, hexadecapole and triaxial deformations, respectively. The spherical energy levels are shown at the left-hand side of the plot, each indicated with the radial quantum number n and the corresponding angular momentum l. In the left panels, the solid lines correspond to four-fold degenerate states ($\Lambda \neq 0$) for axial symmetry. The large gap for $N = 86$ leads to the stable triaxial ground state deformation of $(\varepsilon_2, \varepsilon_4, \gamma) = (0.19, 0.09, 26)$.

Figure 3:
Contour diagrams of the PES for $N = 12, 14, 16, 28, 86, 132, 186$ and 228 in the (ε_2, γ)–plane.
The triaxiality parameter γ is represented by the angle $0° \leq \gamma \leq 60°$. The abszissa corresponds to the quadrupole deformation ε_2 at the minimized hexadecapole deformation ε_4 in each mesh point. $\gamma = 0°$ corresponds to prolate, $\gamma = 60°$ to oblate cluster shapes. The gray-tone scales indicate the relative energies, with the units of each step in the contours given below each diagram.

Figure 4:
Deformation energy surfaces in the $(\varepsilon_2, \varepsilon_4)$–plane for the clusters $N = 78, 112, 122$ and 154. By minimization of the three-dimensional deformation space these clusters are all found to have axial symmetry, with a pronounced minimum at the prolate side.

Figure 5:
Ground state shapes of sodium clusters as a function of cluster size $N \leq 270$. The lowest panel shows the triaxial deformations with $0 \leq \gamma \leq 60°$. For $\gamma = 0°$, the shape is prolate, whereas oblate shapes correspond to $\gamma = 60°$. The two upper panels show the minimized axial quadrupole and hexadecapole deformations $\varepsilon_2(N)$ and $\varepsilon_4(N)$. The sign of ε_4 describes the waist-line development ($\varepsilon_4 > 0$) or its opposite ($\varepsilon_4 < 0$).

Figure 6:
Separation energies $\Delta_1 E(N) = E_{tot}(N-1) - E_{tot}(N)$ as a function of cluster size N for the minimized ground state shapes $(\varepsilon_2, \varepsilon_4, \gamma)$.

Figure 7:
Deformation energies corresponding to one-, two- and three-dimensional minimization of the shapes as a function of the cluster size N. The most dominant deformation effects come from the quadrupole- and hexadecapole contributions, whereas the triaxiality is much too small to reduce the deformations energies with respect to the axial cases significantly.

Figure 8:
The orbital magnetic moments of odd sodium clusters calculated for the KSN potential. Dots display the lowest axial minima and triangles triaxial minima. The quenching of the orbital magnetic moment by triaxial deformation is demonstrated by the vertical lines. The lower panel shows the triaxiality parameter γ.

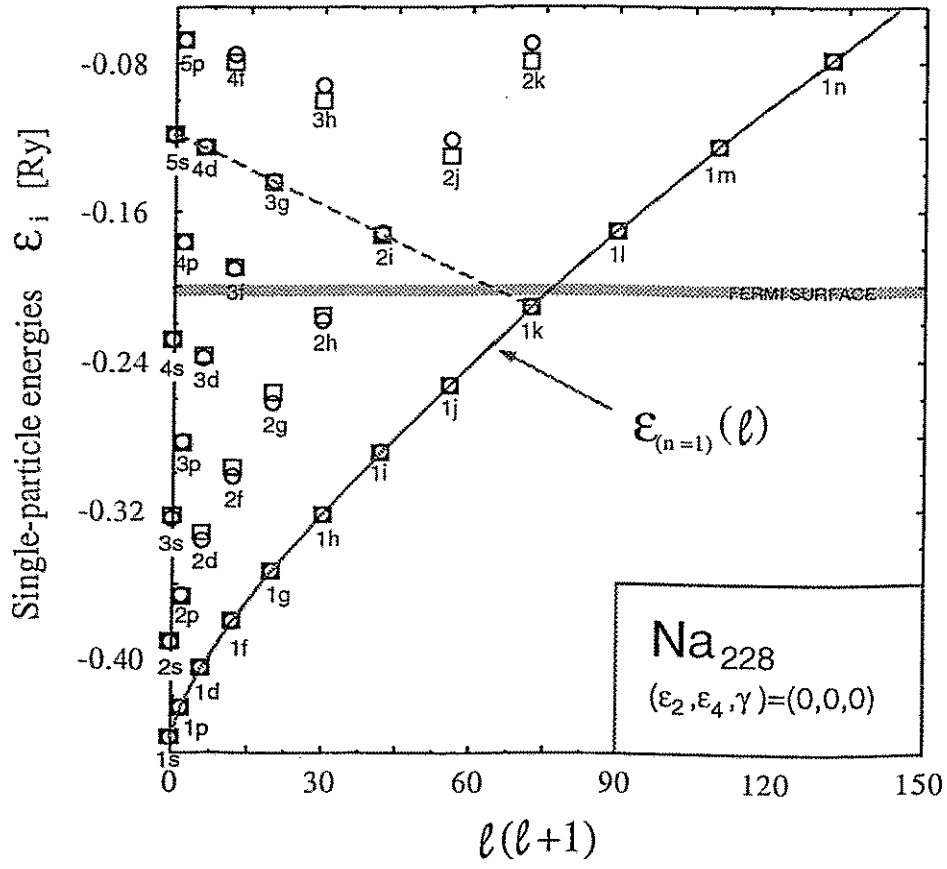
Single-particle energies ε_i [Ry]
-0.08
-0.16
-0.24
-0.32
-0.40
0
30
60
90
120
150
$\ell(\ell+1)$
FERMI SURFACE
$\varepsilon_{(n=1)}(\ell)$
Na_{228}
$(\varepsilon_2, \varepsilon_4, \gamma)=(0,0,0)$
1s
2s 1p
3s 2p 1d
4s 3p 2d 1f
3d 2f 1g
4d 3f 2g 1h
5s 4p 3g 2h 1i
4f 3h 2i 1j
5p 4f 3h 2j 1k
2k 1l
1m
1n

Fig.1

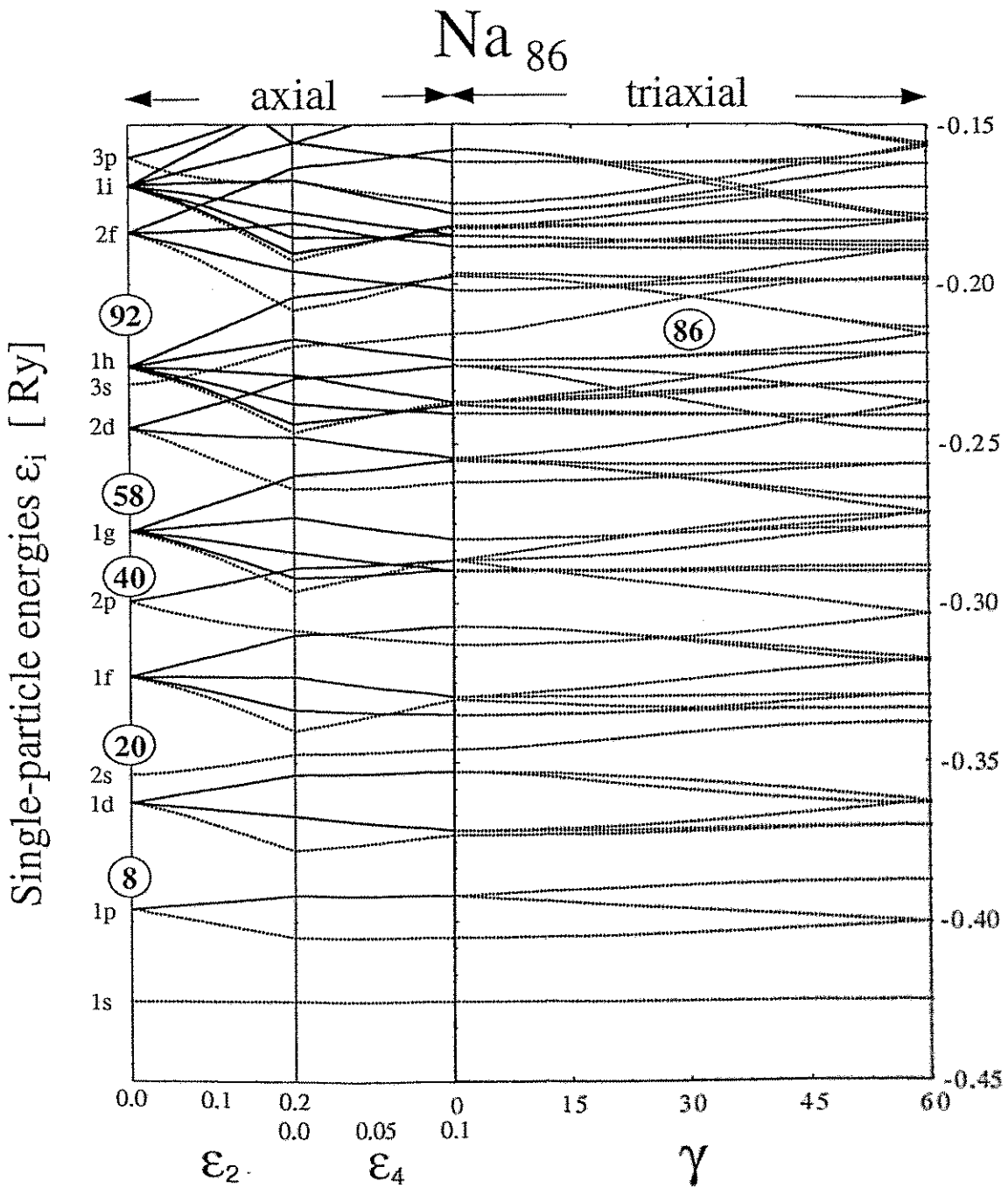

Fig.2

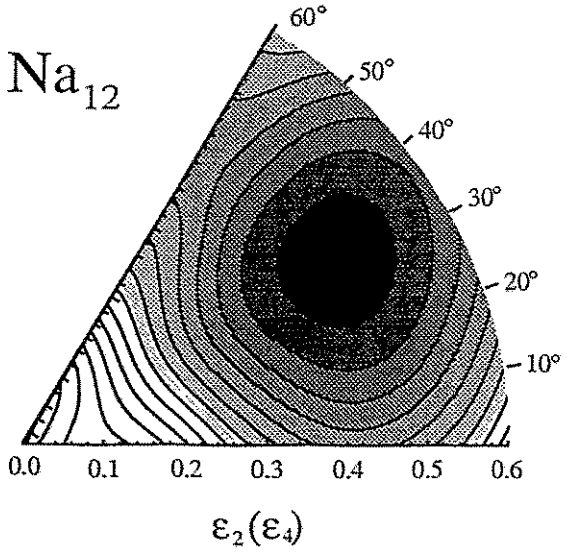

Units 0.045 eV

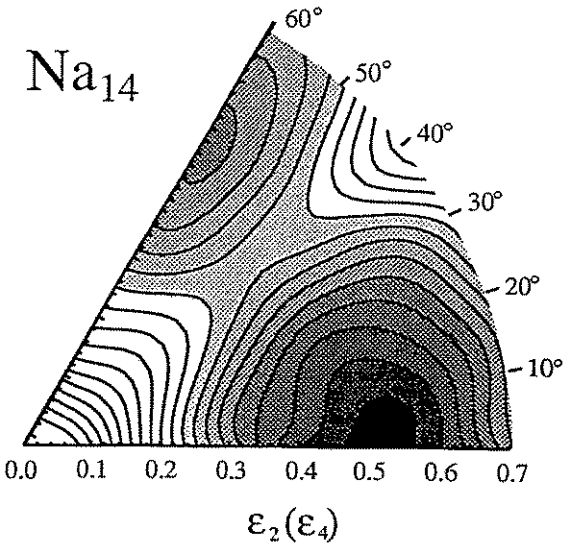

Units 0.051 eV

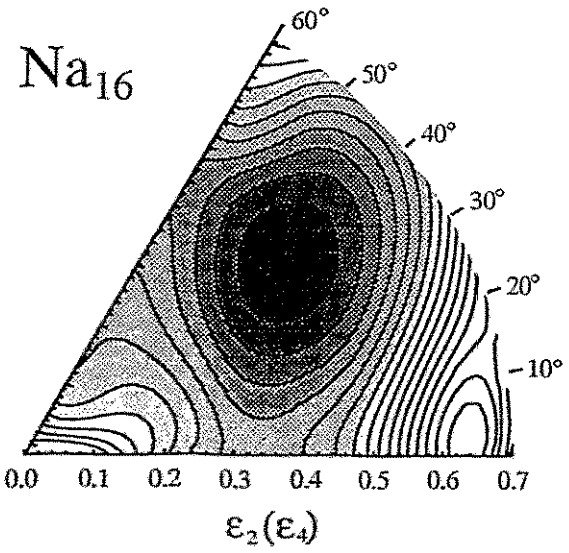

Units 0.025 eV

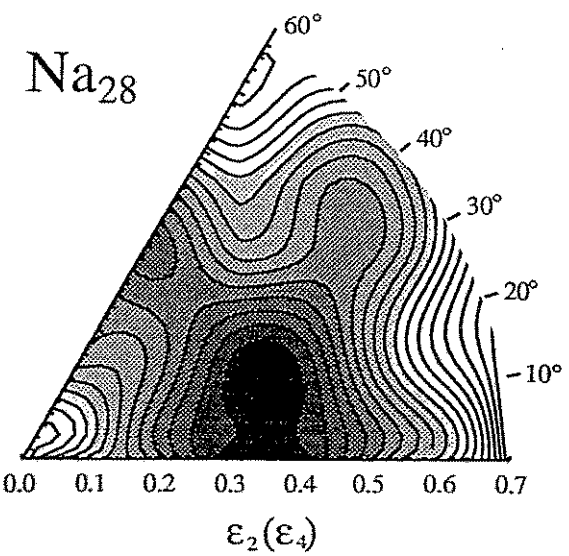

Units 0.046 eV

Fig.3

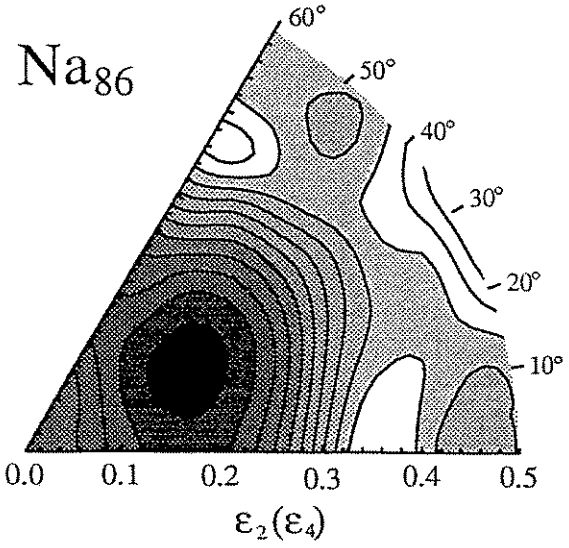

Units 0.09 eV

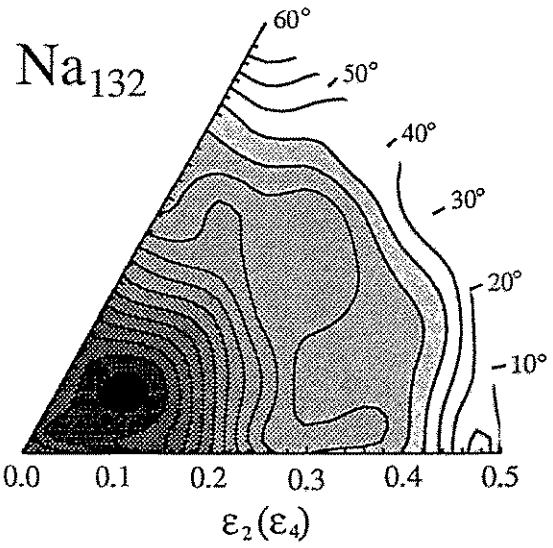

Units 0.09 eV

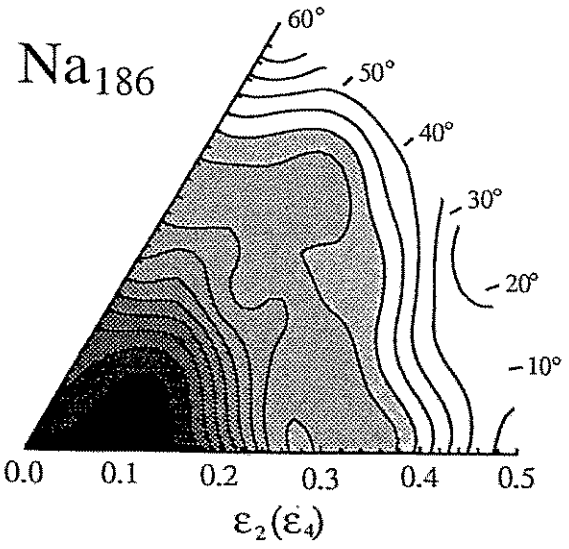

Units 0.13 eV

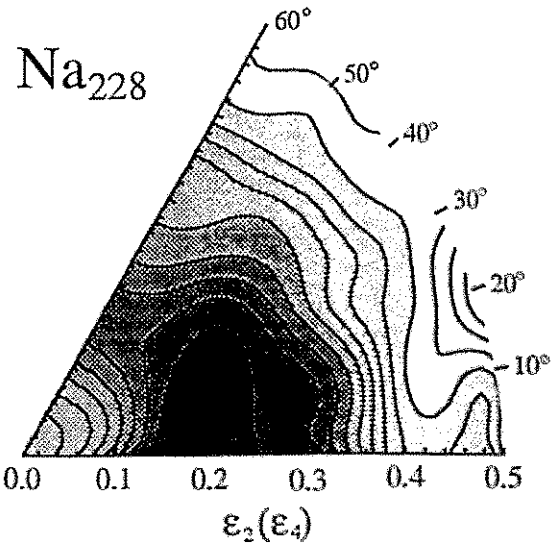

Units 0.13 eV

S M Fiderman et al, Jan. 1995

Fig. 3 (continued)

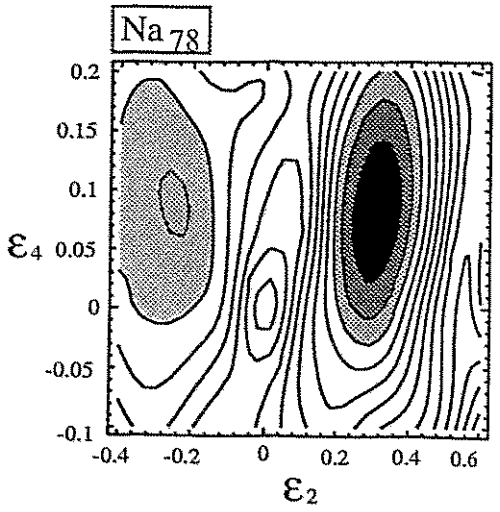

Units: 0.178 eV

prolate $\varepsilon_2 = 0.31$ $\varepsilon_4 = 0.08$

oblate $\varepsilon_2 = -0.25$ $\varepsilon_4 = 0.09$

$E_o - E_p = 0.59$ eV

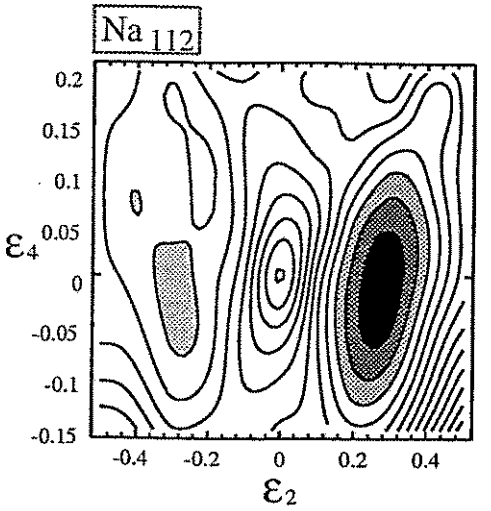

Units: 0.220 eV

prolate $\varepsilon_2 = 0.28$ $\varepsilon_4 = -0.02$

oblate $\varepsilon_2 = -0.40$ $\varepsilon_4 = 0.07$

$E_o - E_p = 0.75$ eV

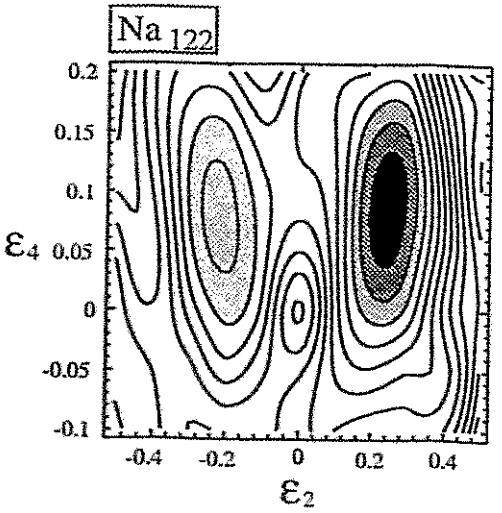

Units: 0.172 eV

prolate $\varepsilon_2 = 0.24$ $\varepsilon_4 = 0.09$

oblate $\varepsilon_2 = -0.22$ $\varepsilon_4 = 0.08$

$E_o - E_p = 0.52$ eV

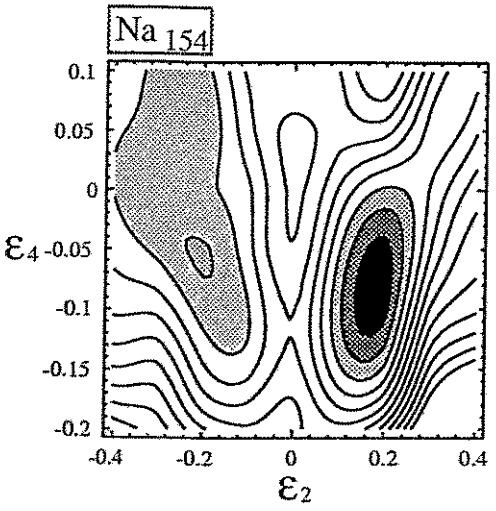

Units: 0.197 eV

prolate $\varepsilon_2 = 0.18$ $\varepsilon_4 = -0.08$

oblate $\varepsilon_2 = -0.20$ $\varepsilon_4 = -0.05$

$E_o - E_p = 0.48$ eV

Fig. 4

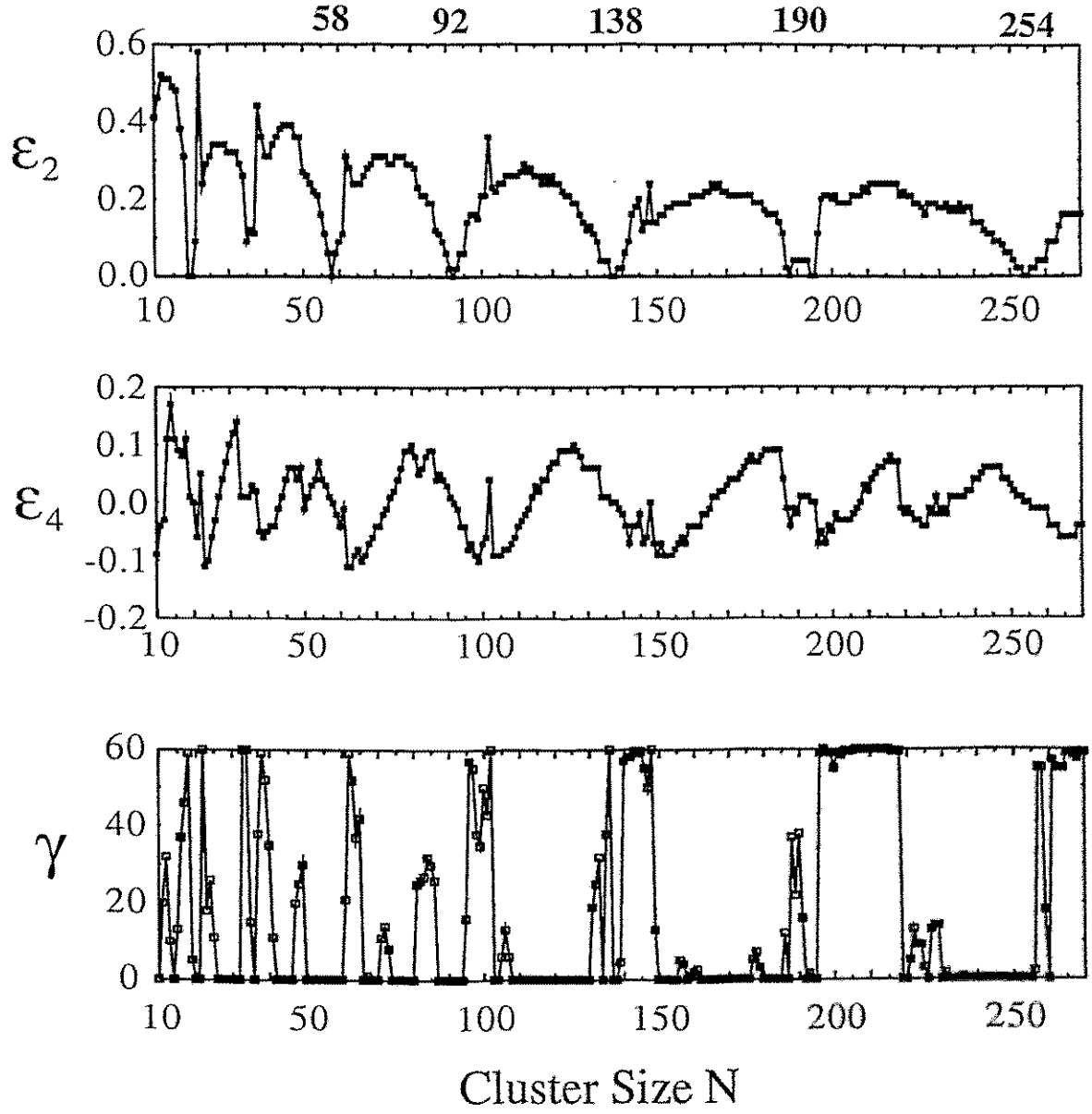
58
92
138
190
254
ε_2
ε_4
γ
Cluster Size N

Fig.5

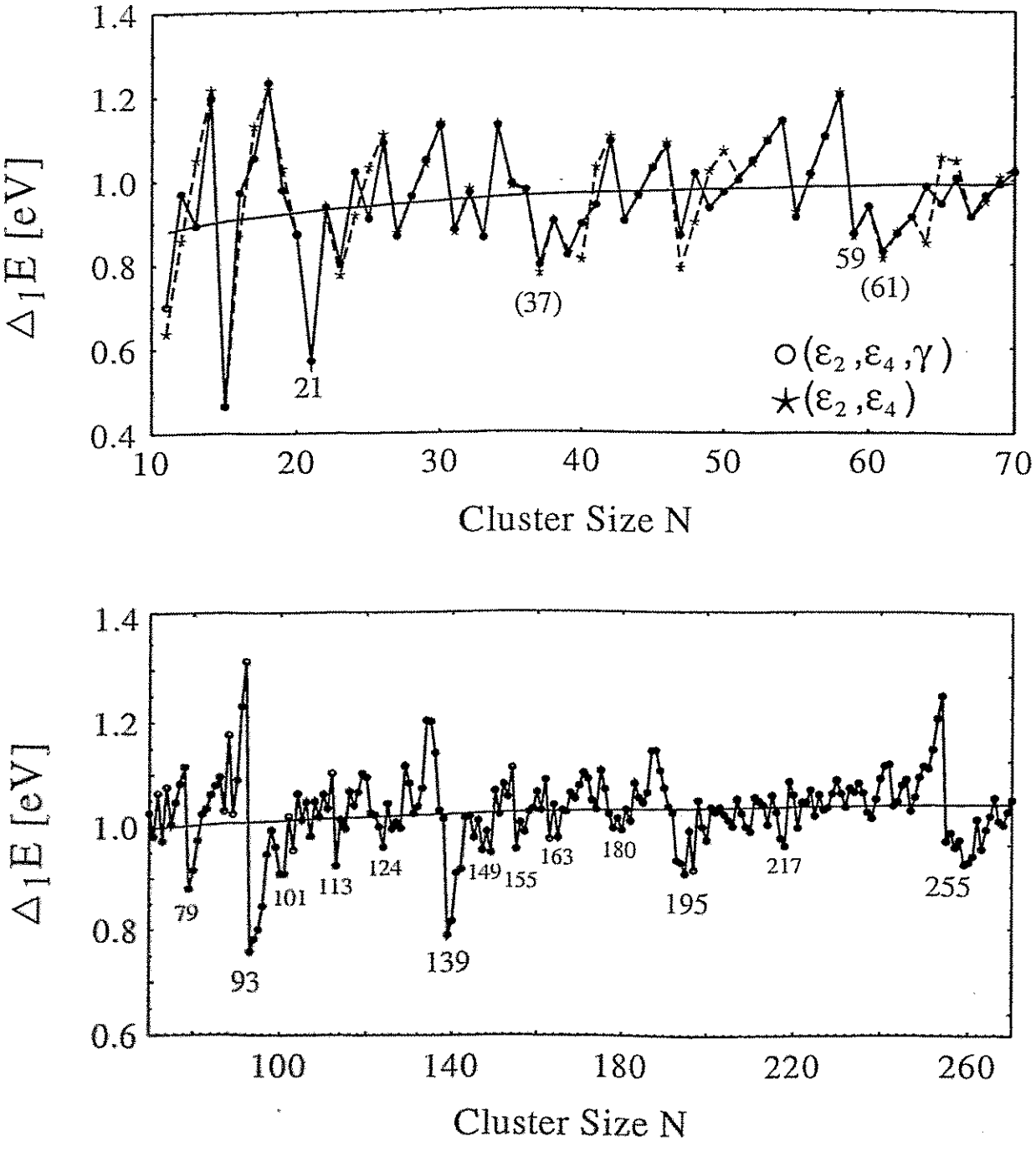
1.4
1.2
1.0
0.8
0.6
0.4
$\Delta_1 E$ [eV]
10
20
30
40
50
60
70
Cluster Size N
21
(37)
59
(61)
○(ε_2, ε_4, γ)
★(ε_2, ε_4)
1.4
1.2
1.0
0.8
0.6
$\Delta_1 E$ [eV]
100
140
180
220
260
Cluster Size N
79
93
101
113
124
139
149
155
163
180
195
217
255

Fig.6

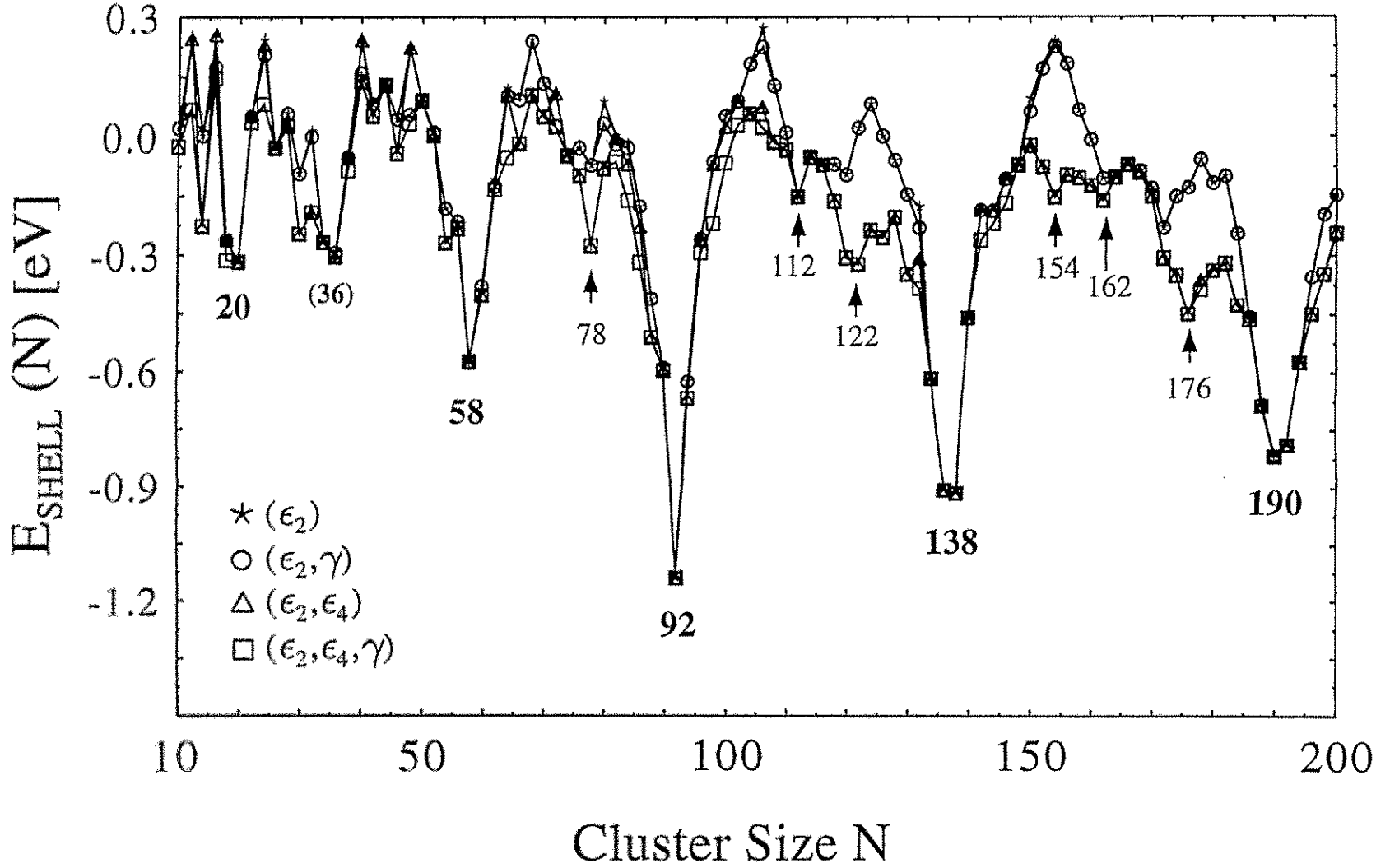
0.3
0.0
-0.3
-0.6
-0.9
-1.2
E_{SHELL} (N) [eV]
10
50
100
150
200
Cluster Size N
★ (ϵ_2)
○ (ϵ_2,γ)
△ (ϵ_2,ϵ_4)
□ (ϵ_2,ϵ_4,γ)
20
(36)
58
78
92
112
122
138
154
162
176
190

Fig. 7

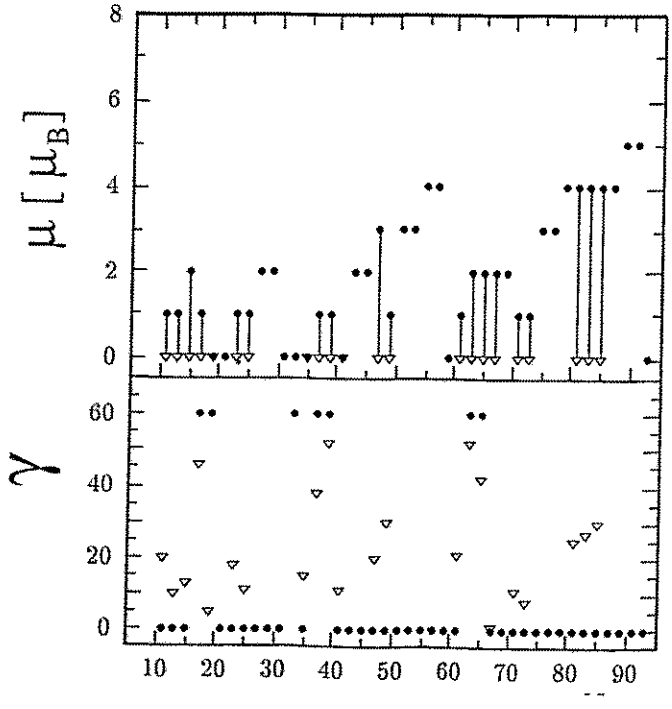

Fig.8